Physica D 35 (1989) 299–317
North-Holland, Amsterdam

COMPUTATIONAL CHAOS – A PRELUDE TO COMPUTATIONAL INSTABILITY

Edward N. LORENZ
Center for Meteorology and Physical Oceanography, Massachusetts Institute of Technology, Cambridge, MA 02139, USA

Received 16 June 1988
Communicated by R.M. Westervelt

Chaotic behavior sometimes occurs when difference equations used as approximations to ordinary differential equations are solved numerically with an excessively large time increment τ. In two simple examples we find that, as τ increases, chaos first sets in when an attractor A acquires two distinct points that map to the same point. This happens when A acquires slopes of the same sign, in a rectifying coordinate system, at two consecutive intersections with the critical curve. Chaotic and quasi-periodic behavior may then alternate within a range of τ before computational instability finally prevails. Bifurcations to and from chaos and transitions to computational instability are highly scheme-dependent, even among differencing schemes of the same order. Systems exhibiting computational chaos can serve as illustrative examples in more general studies of noninvertible mappings.

1. Introduction

Typical systems of nonlinear ordinary differential equations possess general time-dependent solutions that are not readily expressible in terms of familiar functions. Particular solutions are most often sought by numerical means. Solutions of the vector system

$$\mathrm{d}\boldsymbol{X}/\mathrm{d}t = \boldsymbol{F}(\boldsymbol{X}) \tag{1}$$

may be approximated by using Euler's forward-differencing scheme, i.e., by choosing a time increment τ and iterating the system of difference equations

$$\boldsymbol{X}_{n+1} = \boldsymbol{X}_n + \tau \boldsymbol{F}(\boldsymbol{X}_n), \tag{2}$$

or, more commonly, by using some higher-order or more elaborate scheme.

Anyone who has devoted much time to solving nonlinear differential equations numerically has almost surely encountered *computational instability* – a rapid and unbounded amplification of the variables that can occur when τ is too large. Computational instability can often be cured simply by making τ smaller, without otherwise altering the procedure, although in some non-dissipative systems – for example, in eq. (1) when $\boldsymbol{X} \cdot \boldsymbol{F}$ vanishes identically – a blow-up may eventually occur no matter how small τ has been made, if a conventional differencing scheme is used without modification [1].

Even when τ is small enough to ensure computational stability, a simple mapping such as (2) may not be a good approximation to the flow (1) on which it is based. This is, after all, why more elaborate schemes such as higher-order Runge-Kutta schemes have been developed. The disagreement need not be merely quantitative. Solutions that ought to be attracted to stable fixed points, and will be if τ is small enough, may, with a larger τ, approach limit cycles, while solutions that ought to approach limit cycles, as well as those that should approach fixed points, may vary chaotically. We shall refer to chaotic behavior that owes its existence to the use of an excessively large time increment as *computational chaos*.

For definiteness we shall use the term *chaos* to mean the presence, at least throughout a basin of attraction, of sensitive dependence on initial conditions. A prominent consequence of sensitive dependence is that almost all points in the relevant basins lie on aperiodic orbits. This usage, which has become fairly common, seems to have evolved from the use of "chaos" by Li and Yorke [2] to denote the presence of *some* aperiodic orbits, even when almost all points lie on periodic orbits.

It should not surprise us that computational chaos is widespread, since it appears even when eq. (1) is one of the simplest imaginable nonlinear flows – the single equation

$$\mathrm{d}x/\mathrm{d}t = x - x^2 \tag{3}$$

in the single scalar dependent variable x. Eq. (3) possesses the general solution $x = \mathrm{e}^t/(\mathrm{e}^t + c)$, and almost all particular solutions approach either $-\infty$ or the stable fixed point $x = 1$. If we apply the Euler scheme (2), we obtain

$$x_{n+1} = (1+\tau)x_n - \tau x_n^2, \tag{4}$$

a form of the logistic equation whose properties have been recounted many times [3, 4]. Solutions with $0 < x_0 < (1+\tau)/\tau$ correctly approach the fixed point $x = 1$ if $\tau < 2$, but, as τ increases from 2 to 3, the general solution first undergoes period doubling and then enters a range of chaotic behavior, generously interspersed with periodic windows. As τ passes 3, true computational instability sets in.

Nevertheless, neither computational instability nor computational chaos is inevitable. For example, when the Euler scheme is applied to the scalar equation

$$\mathrm{d}x/\mathrm{d}t = -x/(1+x^2), \tag{5}$$

chaos sets in at the culmination of a period-doubling sequence, when $\tau = 5.309$, but computational instability never develops. We shall presently encounter a simple example where computational instability sets in as soon as the fixed points become unstable, with no intervening chaotic behavior.

Descriptions of particular instances of computational chaos date back at least to the pioneering work of Stein and Ulam [5] on nonlinear transformations, performed soon after digital computers had become powerful enough to permit one to make a large number of runs, each consisting of thousands or perhaps hundreds of thousands of iterations. Their approach is indirect; having found a mapping

$$\boldsymbol{X}_{n+1} = \boldsymbol{G}(\boldsymbol{X}_n) \tag{6}$$

that produces a chaotic attractor, they effectively convert the chaos to computational chaos by treating the mapping as the result of applying the Euler scheme to the flow

$$\mathrm{d}\boldsymbol{X}/\mathrm{d}t = \boldsymbol{G}(\boldsymbol{X}) - \boldsymbol{X}, \tag{7}$$

with $\tau = 1$.

It thus appears that any mapping

$$\boldsymbol{X}_{n+1} = \boldsymbol{H}(\boldsymbol{X}_n, \alpha) \tag{8}$$

is equivalent, for a fixed value of a scalar parameter α, to some mapping of the form (2), with a fixed τ. It does not follow, however, that a *sequence* of mappings, produced by varying α in (8), is in general equivalent to any sequence produced by varying τ in (2). In particular, transitions to computational chaos are conceivably more specialized than transitions to chaos in general.

More recently Yamaguti and Ushiki [6] have applied centered and mixed differencing schemes, which express $\boldsymbol{X}_{n+1}$ in terms of $\boldsymbol{X}_n$ and $\boldsymbol{X}_{n-1}$, to eq. (3), and, with the mixed scheme, have obtained a mapping equivalent to that of Hénon [7], which possesses a chaotic range. Whitehead and MacDonald [8] have produced chaos by applying the Euler differencing scheme to a two-dimensional flow introduced by Burgers [9] as a model of certain features of fluid turbulence. On the theoretical side, Yamaguti and Matano [10] have

shown that if the Euler scheme is applied to a scalar equation having both stable and unstable fixed points (as does eq. (3), for example), a sufficiently large τ will produce chaos in the sense of Li and Yorke [2]. Ushiki [11] has shown that the application of a centered differencing scheme to eq. (3) produces chaos, in the same sense.

Aside from simply being different equations from (1), and hence possessing different properties, eq. (2), and other approximations to (1) where $\boldsymbol{X}_{n+1}$ is given in terms of $\boldsymbol{X}_n$, generally differ from (1) in an important qualitative way; they are not uniquely invertible, although they may be invertible for special values of τ. They may also be invertible over certain regions, and in particular, over an attractor. In this work we shall be concerned with differencing schemes that produce noninvertible mappings. Some schemes, including the centered and mixed schemes used in [6], produce invertible mappings.

A sufficient condition that a noninvertible mapping, whether or not it is identified with a numerical integration scheme, be chaotic is that two distinct points P and P^* in an attractor A map to the same point P_1 in A. A non-rigorous argument is that if R and R^* are regions containing P and P^*, with diameters much smaller than the distance from P to P^*, the sequence of forward images of P_1, or of some point in A close to P_1, must eventually enter R and R^*, and must enter one of these regions, say R, before the other. If there is no sensitive dependence on initial conditions, the next image in the sequence will lie near P_1, and the subsequent images will lie near the earlier images, thus continually reentering R and avoiding R^*, in contradiction to the previous statement.

The proposition seems so apparent that we suspect that it is well known, but we have not discovered a specific reference to it. Similar reasoning leads to the conclusion that a sufficient condition that an invertible mapping or a flow be chaotic is that two distinct orbits in an attractor approach each other asymptotically.

We should add that, even for noninvertible mappings, noninvertibility on A is not a necessary condition for chaos. There are plenty of invertible mappings, including the Hénon mapping [7], that are chaotic. A small modification of such a mapping can presumably leave it invertible and chaotic on A while rendering it noninvertible somewhere else.

The principal purpose of this work is to examine the progression from good to poor and possibly chaotic approximations and then to computational instability when various differencing schemes are applied with increasingly large time increments to simple but otherwise typical flows. We shall be particularly concerned with the precise onset of chaos and its possible coincidence with the acquisition, by an attractor, of two points that map to the same point. We shall also be concerned with the precise onset of computational instability. A second purpose is to emphasize that the introduction of rather large time increments into otherwise routine numerical integrations can offer a handy means of creating chaos, when one is interested in chaos for its own sake. We shall choose examples where the correct long-term behavior of the original flow can be ascertained without recourse to numerical integration. We are not aware of any comprehensive treatment of computational chaos, nor is our account intended to be comprehensive.

2. A system with fixed-point attractors

Some time ago we introduced the system

$$\mathrm{d}X/\mathrm{d}t = -\sigma X + \sigma Y, \tag{9a}$$

$$\mathrm{d}Y/\mathrm{d}t = -XZ + \rho X - Y, \tag{9b}$$

$$\mathrm{d}Z/\mathrm{d}t = XY - \beta Z, \tag{9c}$$

where σ, ρ, β are positive constants, as a highly truncated model of fluid convection [12]. The system has a fixed point O at the origin, which is unstable when $\rho > 1$. In that event there are two additional fixed points Q and Q' differing only in the signs of X and Y; these are unstable when

$\sigma > \beta + 1$ and $\rho > \sigma(\sigma + \beta + 3)/(\sigma - \beta - 1)$. Orbits may then be chaotic, shuttling back and forth from the vicinity of Q to that of Q' at seemingly irregular intervals. Time series of X and Y look much alike, but those of Z look more like those of X^2 and Y^2. The system has been intensively studied from the topological as well as the analytical point of view.

For the leading example in the present study we choose the limiting form of eqs. (9) as $\sigma \to \infty$ while ρ and β remain fixed, i.e., we discard (9a) and replace X by Y in (9b) and (9c). We then note that, if $\beta \neq 1$, we can reduce β to 1 simply by rescaling the variables and the remaining constant; this is not true of the original equations (9). Setting $\beta = 1$, letting $a = \rho - 1$, and denoting the dependent variables by x and y instead of Y and Z, we obtain the system

$$\mathrm{d}x/\mathrm{d}t = ax - xy, \tag{10a}$$

$$\mathrm{d}y/\mathrm{d}t = -y + x^2. \tag{10b}$$

We shall consider cases where $a > 1/8$.

Infinitesimal departures (ξ, η) from (x, y) are governed by the system

$$\frac{\mathrm{d}}{\mathrm{d}t}\begin{pmatrix}\xi\\ \eta\end{pmatrix} = \begin{pmatrix}a-y & -x\\ 2x & -1\end{pmatrix}\begin{pmatrix}\xi\\ \eta\end{pmatrix}, \tag{11}$$

whose characteristic equation is

$$\lambda^2 + (1 - a + y)\lambda + (2x^2 - a + y) = 0. \tag{12}$$

Introducing the values $x^2 = a$, $y = a$ at Q or Q' we find, since $a > 1/8$, that the roots of (12) are complex, and the Lyapunov exponents l_1 and l_2 (with $l_1 \geq l_2$), which in this case are the real parts of the roots, both equal $-1/2$.

Upon approximating eqs. (10) with the first-order scheme (2), we obtain

$$x_{n+1} = (1 + a\tau)x_n - \tau x_n y_n, \tag{13a}$$

$$y_{n+1} = (1 - \tau)y_n + \tau x_n^2. \tag{13b}$$

Eqs. (13) are equivalent to those studied in [8].

For a fixed value of a, we shall be interested in three critical values of τ. These are τ_a, the lower limit of values of τ for which Q and Q' are unstable, τ_b, the lower limit of values for which chaos is present, and τ_c, the lower limit of values for which computational instability occurs.

Infinitesimal perturbations (ξ, η) are now governed by

$$\begin{pmatrix}\xi\\ \eta\end{pmatrix}_{n+1} = \begin{pmatrix}1 + a\tau - \tau y & -\tau x\\ 2\tau x & 1 - \tau\end{pmatrix}_n \begin{pmatrix}\xi\\ \eta\end{pmatrix}_n, \tag{14}$$

whose characteristic equation is

$$\lambda^2 - T_n\lambda + \Delta_n = 0, \tag{15}$$

where T_n and Δ_n are the trace and the determinant of M_n, the square matrix in (14). Again the roots of (15) are complex when x_n and y_n assume their values at Q or Q'. Since we are now dealing with a mapping, the stability of Q and Q' depends upon the real parts of the logarithms of the roots. We find that l_1 and l_2, expressed in inverse time units, both equal $[\log(1 - \tau + 2a\tau^2)]/(2\tau)$, which appropriately approaches $-1/2$ as $\tau \to 0$ but vanishes when $\tau = 1/(2a)$; thus $\tau_a = 1/(2a)$.

At $\tau = \tau_a$ there is a Hopf bifurcation, and, if this is supercritical, the attractors just beyond τ_a should be quasi-elliptical limit cycles. Since Q and Q' are no longer attractors, their degree of stability does not determine l_1 and l_2. We can estimate l_1 and l_2 numerically by forming the product $M_{N-1}M_{N-2}\cdots M_0$ for some large N and solving the characteristic equation. If the roots are real, the product matrix is likely to be nearly singular, making the estimate of l_2 suspect, and we can independently estimate the sum $l_1 + l_2$ from the product $\Delta_{N-1}\Delta_{N-2}\cdots\Delta_0$.

As for the noninvertibility, given x_{n+1} and y_{n+1}, we find from (13) that x_n satisfies

$$\tau^2 x^3 - \tau(y_{n+1} - cb)x - cx_{n+1} = 0, \tag{16}$$

where $b = (1 + a\tau)/\tau$ and $c = 1 - \tau$. Eq. (16) has two equal roots when (x_{n+1}, y_{n+1}) lies on the

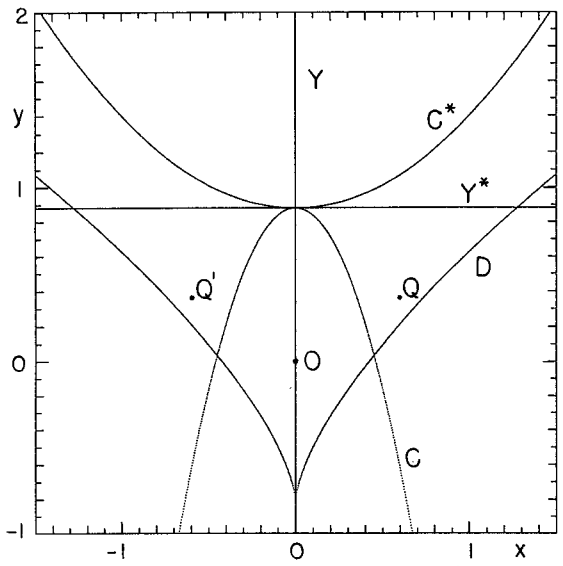

Fig. 1. The critical curve C and its image D and the other inverse image C^* of D, the y-axis Y and its inverse image Y^*, and the fixed points O, Q, and Q', for eqs. (13) with $a = 0.36$ and $\tau = 1.92$.

curve D (see fig. 1) given by

$$4\tau(y - cb)^3 = 27c^2x^2. \tag{17}$$

Evidently D possesses a downward-pointing cusp on the y-axis (unless $\tau = 1$). Points above D have three inverse images, while those below have only one.

The double inverse image of D is the parabolic critical curve C obtained by setting $\Delta = 0$, and hence given by

$$c(y - b) = 2\tau x^2. \tag{18}$$

Points immediately above or below C (and not on the y-axis) map to points above D, so that small regions intersecting C are effectively folded over on D by the mapping, and are highly compressed in the direction normal to D. The remaining inverse image of D is the parabola C^* given by

$$4c(y - b) = -\tau x^2. \tag{19}$$

Only points below C^* if $\tau < 1$, or above C^* if $\tau > 1$, map to points below D. The y-axis Y maps onto itself; the other inverse images of the portion of Y above D are the positive and negative halves of the horizontal line Y^* where $y = b$. Points above Y^* map to the opposite side of Y.

Fig. 1 shows the curves C, D, C^*, Y, and Y^*, and also the points O, Q and Q', when $a = 0.36$ and $\tau = 1.92$. The picture is qualitatively similar for other values of $\tau > 1$. When $\tau < 1$, the positions of C and C^* are interchanged.

Given a point (x, y) above D, the remaining points (x^*, y^*) having the same forward image as (x, y) may be found by first solving the quadratic equation

$$\tau x^{*2} + \tau x x^* - c(y - b) = 0, \tag{20a}$$

obtained by dividing out the known root (x, y) from (16), and then observing from (13b) that

$$c(y^* - y) + \tau(x^{*2} - x^2) = 0. \tag{20b}$$

As we have noted, the system will be chaotic if some point (x, y), and one of the corresponding points (x^*, y^*) distinct from (x, y), both lie on an attractor A. Equivalently, if A^* is the set of points (x^*, y^*) that satisfy (20) with (x, y) on A, the system will be chaotic if A and A^* intersect at a point not on C.

3. A route to chaos

It is not the main purpose of this paper to present an exhaustive treatment of one more dynamical system. Nevertheless, we feel that a fairly detailed analysis may constitute the most effective exposition. We shall examine eqs. (13) with $a = 0.36$.

Fig. 2(a) shows the variations of l_1 and l_2 with τ, up to τ_c ($= 2.073$), where computational instability sets in, as resolved by numerical estimates at intervals of 0.0025. In our estimates we let $N = 1000$ and choose distances $\delta_1 = 10^{-5}$ and $\delta_2 = 10^{-2}$. We start from a point near Q and perform N iterations to reduce transient effects, ending at (x_0, y_0). We then base our estimates on N itera-

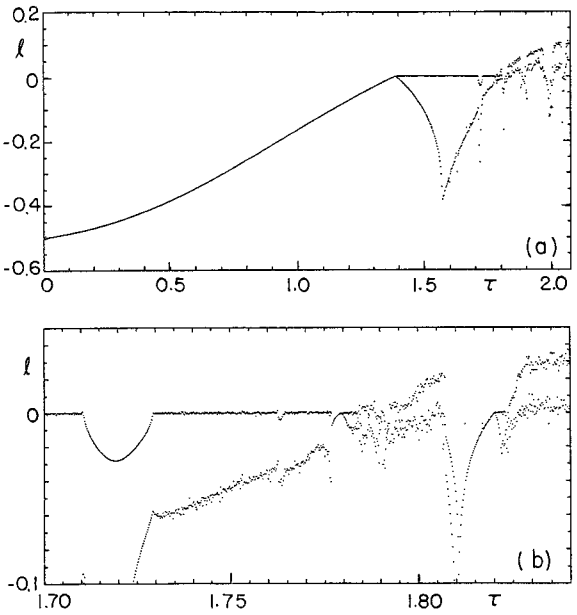

Fig. 2. (a) Numerically estimated values of the Lyapunov exponents l_1 and l_2 ($l_1 \geq l_2$) for values of τ from 0 to τ_c ($= 2.073$) at intervals of 0.0025, for eqs. (13) with $a = 0.36$. (b) The same as (a), except for values of τ from 1.7 to 1.84 at intervals of 0.0002.

tions from (x_0, y_0), with the following modifications: if $\delta(x_m, y_m; x_0, y_0) < \delta_1$ for some $m < N$, where δ is the distance between two points, we stop, and base our estimate on only m iterations, assuming the solution to be periodic of period m; if instead $\delta(x_N, y_N; x_0, y_0) > \delta_2$, we continue until $\delta(x_n, y_n; x_0, y_0) < \delta_2$ for some $n > N$, or until $n = 2N$, and base our estimate on n iterations.

For $\tau < \tau_a$ ($= 1.389$), l_1 and l_2 are negative and equal, in agreement with the theory. Beyond τ_a there is a range where $l_1 = 0$ and $l_2 < 0$, suggesting a limit cycle. As τ nears 1.8, positive values of l_1 appear, implying chaos. Both the limit-cycle range and the chaotic range possess periodic windows. In fig. 2(b) the resolution has been increased to 0.0002 for the range 1.7 to 1.84, which includes the critical value τ_b. A periodic window of period 14 near 1.72 and one of period 9 near 1.81 stand out, while additional narrower windows are resolved. Chaos is prominent when $\tau = 1.8$, but is detectable below 1.785.

The windows are inevitable. Assuming that within a range of τ there is a closed invariant curve, which may be a limit-cycle attractor for some values of τ, and which is continuously deformed as τ varies, the mapping of this curve onto itself will be equivalent to the much studied map of the circle, described in textbooks [13, 14]. A basic result is that between any two values of τ for which the entire curve is the attractor, there must be a periodic window of finite width. Most of the windows are too narrow to be resolved by computation schemes that do not deliberately seek them. Nevertheless, there cannot be a continuum of values of τ with limit-cycle attractors, bounded above by τ_b. At most there may be a sequence of such values of τ, approaching τ_b. We have chosen the case $a = 0.36$ for study partly because of the scarcity of wide windows near τ_b.

Fig. 3 shows attractors A for four selected values of τ. In each case there is also a second attractor A' – the mirror image of the first in Y. Each picture was produced by plotting a long succession of points in a single numerical solution.

The first attractor is the anticipated ellipse, already somewhat distorted. The second, despite its rough appearance, is topologically still an ellipse. The apparent cusps are actually points of extreme curvature. The third, although suggestive of the second, is chaotic, and may be seen under magnification to possess a Cantor-set structure. The fourth is visibly chaotic, and, despite the hole surrounding Q, appears to be fully two-dimensional in the region it covers. Because fig. 3(d) contains a finite number of points, the more frequently visited portions of A appear more heavily shaded. Evidently $l_1 + l_2 > 0$, so that the mapping is expanding, and in fact even $l_2 > 0$. It is only because two regions can map onto the same region that the solution can remain bounded. Superficially A resembles the projection on a plane of the attractor of a three-variable invertible system whose fractional dimension exceeds two.

The key to the explanation of the similarities as well as the differences in figs. 3(b) and 3(c) lies in fig. 3(d), where A possesses smooth boundaries

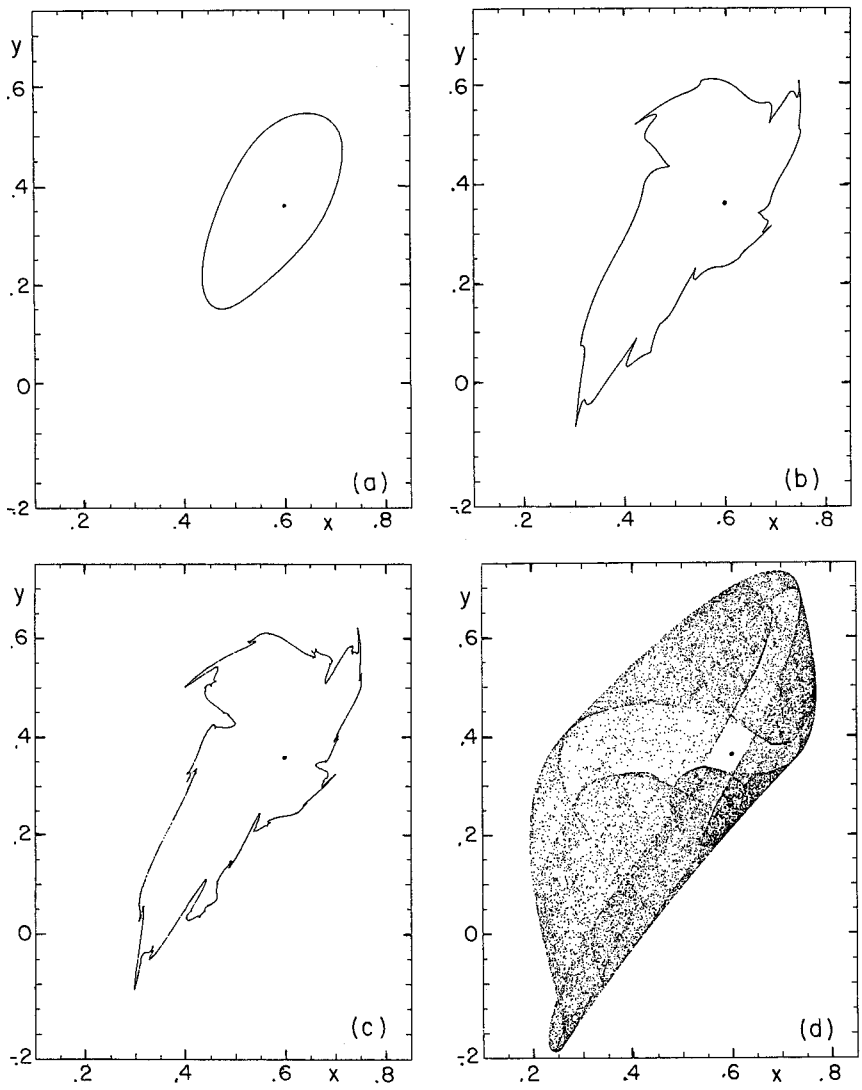

Fig. 3. (a) The attractor A of eqs. (13) with $a = 0.36$ and $\tau = 1.50$. The mirror image A' of A in the y-axis is a second attractor. The point at (0.6, 0.36) is Q. (b) The same as (a), except that $\tau = 1.775$. (c) The same as (a), except that $\tau = 1.785$. (d) The same as (a), except that $\tau = 1.92$.

despite its chaotic interior; clearly the lower right boundary lies on D. Assuming only that A occupies and fills a restricted region that intersects C but not Y^*, the segment of C contained in A must map onto a segment of D, while points on either side of C will map to points above D. The remaining boundary segments of A and the prominent interior discontinuities in shading lie on forward images of D. Fig. 4 shows the first five forward images of the segment of C that extends from its first intersection with its third image to its intersection with its first image; the outlines of A have been aptly recaptured.

The sequence of attractors displayed in fig. 3 is qualitatively much like one encountered by Stein and Ulam [5] in their study of cubic transformations; their attractor with $\tau = 1$ fills a two-dimensional annular region. A sequence exhibited by

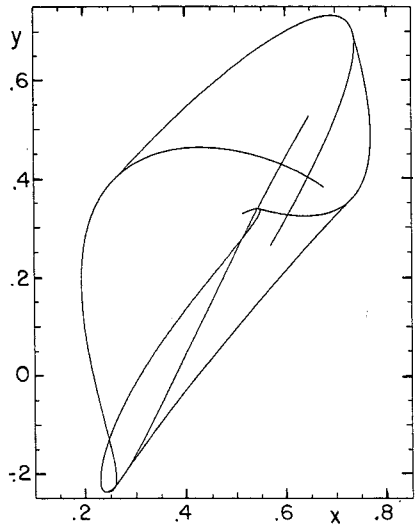

Fig. 4. A superposition of the first five images of the portion of the curve C between its first positive intersection with its third image and its positive intersection with its first image, for eqs. (13) with $a = 0.36$ and $\tau = 1.92$.

Beddington et al. [15], obtained from a predator–prey model formulated as a transcendental mapping, resembles our sequence even more closely. Their attractors range from quasi-ellipses to one that fills a two-dimensional region and possesses a smooth outer boundary, presumably composed of segments of forward images of a critical curve.

Returning to the Hopf bifurcation at τ_a, we anticipate that the curve forming A, originally an infinitesimal ellipse, will expand, ultimately pushing across C, even though the continuity of the expansion will be broken by minuscule periodic windows. The images of its points of intersection with C will lie on D, while the remainder of A will lie above D; thus A must possess two protuberances or bumps. The forward images of these bumps must be additional bumps. As A continues to expand, the bumps may become more pronounced, and bumpy portions of A may intersect C, giving rise to still more bumpiness.

In fig. 5(a) we have superposed segments of C and D on the attractor of fig. 3(b), where $\tau = 1.775$. One intersection with C is labeled 0, and its first 37 forward images are labeled from 1 to 37. Image 1, which must lie on D, is at the peak of a

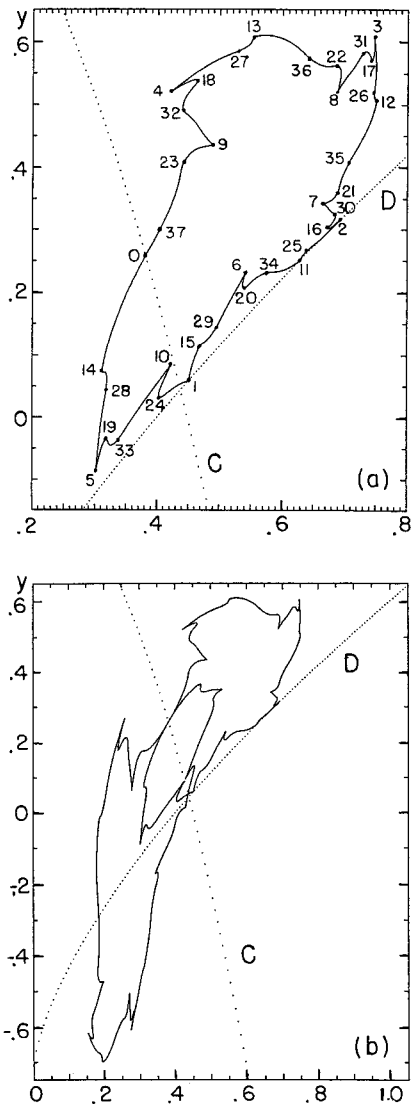

Fig. 5. (a) An enlargement of the attractor A of fig. 3(b), showing portions of the curves C and D. The numbers indicate images of the intersection of A with C that is numbered 0. (b) The attractor A of fig. 3(b) and the portion of the corresponding set A^* that intersects A on C.

noticeable bump, and, because the bump is close to C, its image is compressed in the direction normal to D and appears as an apparent cusp at image 2. We find, in fact, that most of the 37 images correspond to the peaks of visible spikes or bumps, while together they nearly exhaust the visible irregularities of A. Images of the other

intersection of A with C are less prominent; one occurs at the bump between the points numbered 19 and 33.

Fig. 5(b) shows the same attractor A and the piece of A^* (see eqs. (20)) below Y^*. Evidently A^* is like a circus-mirror image of A in C. The only intersections of A and A^* are on C, but only minor additional distortions of A would be needed to produce intersections with A^* off C. To pursue this matter it is convenient to introduce a "rectifying" coordinate system (x_r, y_r) in which C becomes a straight line, and A and A^* become exact mirror images in C. It suffices to let $x_r = (x - x^*)/2$ and $y_r = (y + y^*)/2$, whereupon C becomes the y_r-axis. We may wish to follow this transformation by a rotation. Fig. 6(a) shows A, again for $\tau = 1.775$, in rectifying coordinates, after a rotation that makes C the x_r-axis. One need not actually draw the mirror image of A to see that it intersects A only on C.

If A is still quasi-elliptical when it first pushes across C, its two intersections with C will slope in opposite directions. A sufficient condition for A to intersect A^* off C is that its two intersections with C acquire slopes of the same sign, or, if additional crossings appear, that two consecutive crossings have slopes of the same sign. A slight modification of A, as τ increases, could easily change the sign of the left-hand slope in fig. 6(a). What actually happens, however, is that the protuberance that is just reaching C in fig. 6(a) (near $(-0.1, 0)$) pushes across C, and soon afterward the slope of its right-hand crossing changes sign. Fig. 6(b) indicates that this has already happened when $\tau = 1.785$.

Fig. 7(a) is an enlargement, with additional horizontal stretching, of a neighborhood of the protuberance in fig. 6(b) (enclosed by the larger rectangle), while fig. 8(a), which enlarges the lower left corner of fig. 7(a), with still more horizontal stretching, leaves no doubt that the slope at the crossing marked 0 has changed its sign. It follows that A and A^* must intersect somewhere off C; this they do at the points labeled 00 and 000. The forward image of the portion of A in fig. 7(a)

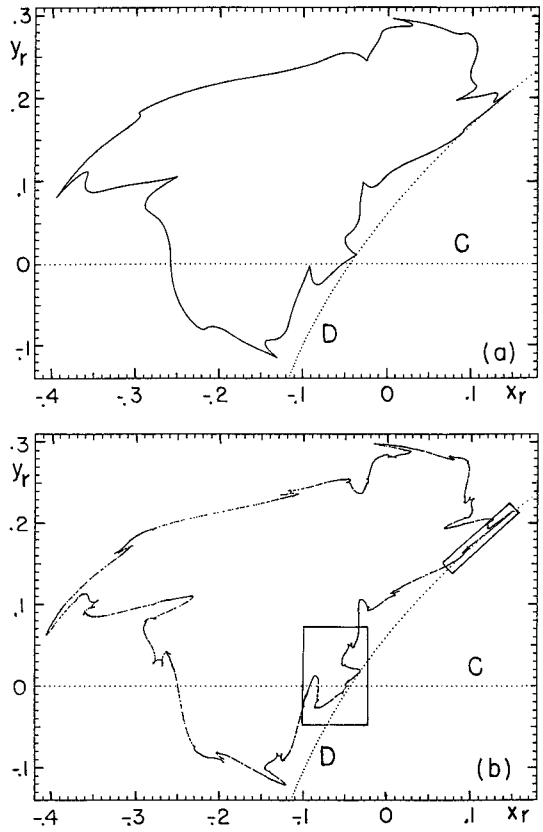

Fig. 6. (a) The attractor A of eqs. (13) with $a = 0.36$ and $\tau = 1.775$, and portions of the curves C and D, in rectifying coordinates. (b) The same as (a), except that $\tau = 1.785$. The small rectangles indicate the regions that have been enlarged in fig. 7.

should then look much like fig. 7(a), but with C replaced by D, and with the value of y_r squared. It should therefore be tangent to D at the image of 0, and should intersect itself at the common image of 00 and 000, whence it should contain a small loop. Fig. 7(b) shows the appropriate portion of fig. 6(b) (enclosed by the smaller rectangle), enlarged, rotated so as to make D quasi-horizontal, and then stretched vertically, while fig. 8(b) enlarges the lower left corner of fig. 7(b). The anticipated loop appears and is labeled 1.

Just above loop 1 there is a rather similar loop, labeled 38. This is of course the image of the loop below 0 in figs. 7(a) and 8(a), labeled 37, but it also proves to be the 37th image of loop 1, or the

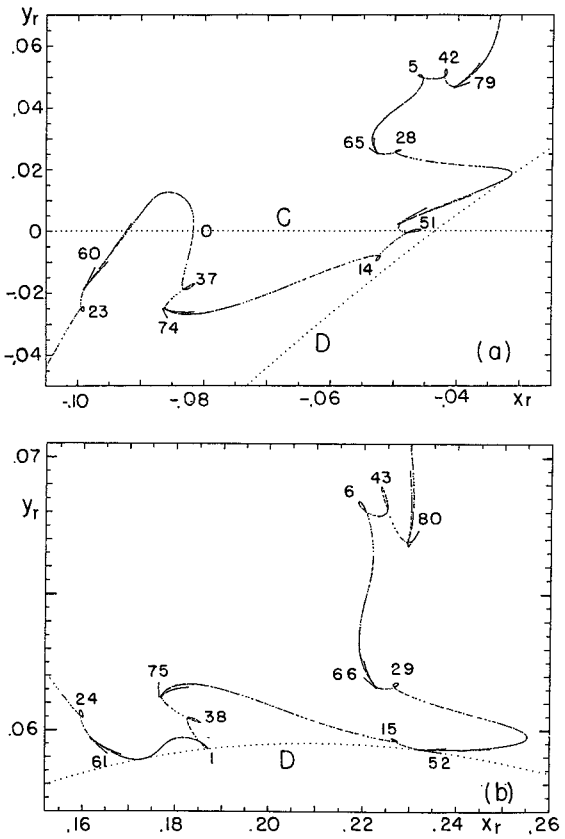

Fig. 7. (a) Enlargement of the portion of fig. 6(b) enclosed by the larger rectangle, followed by additional horizontal stretching. The numbers indicate images of the intersection of A with C that is numbered 0. (b) Enlargement of the portion of fig. 6(b) enclosed by the smaller rectangle, followed by rotation through an angle $\tan^{-1}(-10/9)$ and additional vertical stretching. The numbers indicate images of the intersection of A with C in fig. 7(a) numbered 0. Note that because of the rotation the values of x_r and y_r differ from those in fig. 6(b).

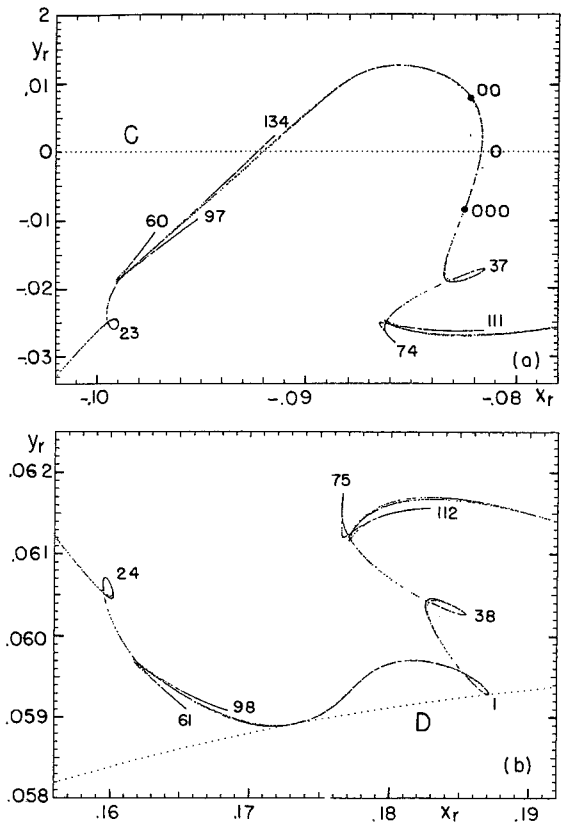

Fig. 8. (a) An enlargement of the lower left portion of fig. 7(a), followed by more horizontal stretching. The points labeled 00 and 000 have the same forward image. (b) An enlargement of the lower left portion of fig. 7(b).

38th image of crossing 0 – hence the label. Loops 23 and 24 also appear in figs. 8(a) and 8(b), while other labeled loops appear in figs. 7(a) and 7(b).

We may ask, if loop 1 is the "original" loop and the other loops are simply its images, why figs. 7(b) and 8(b) do not also contain a loop 75 somewhat above loop 38. The answer is that loop 51 falls on top of C, as seen in fig. 7(a), producing additional intersections of A and A^* near but not on C. What would be loop 52 is therefore something more complicated than a loop, but it is also so compressed in the direction normal to D that it shows up in fig. 7(b) as a short antenna virtually lying on D. We have labeled it 52, and have labeled its forward images, which also resemble antennae. Antenna 75 is indeed prominent in fig. 8(b), as is its 37th image, antenna 112, while in fig. 8(a) antennae 60, 97, and 134 are resolved. The steady increase in the lengths of the antennae that appear to emanate from the same point, as their indices increase by 37, clearly reveals the sensitive dependence on initial conditions, implied by the positive value of l_1, while the tendency of the antennae to lie ever closer to the "main curve" as they stretch out reveals that this "curve" is actually an infinite complex of curves. Note that antenna 134 crosses C, leading to still more complicated fine structure.

We have thus accounted for all of the resolved features in figs. 3(b) and 3(c) and their enlargements in terms of intersections of A with C. For somewhat larger values of τ the loops would be larger and more easily seen, but there would also be a greater tendency for them to overlap, thereby confusing the analysis. We feel that by examining the case $\tau = 1.785$ we have virtually caught chaos in the act of forming. Evidently τ_b is slightly below 1.785.

Catching the exact onset of chaos is more involved. In the range of τ where an invariant closed curve exists, each window begins and ends in a saddle–node bifurcation; the window of period 14 between 1.71 and 1.73 in fig. 2(b) is a typical example. Fig. 2(b) also shows a narrower window of period 37, beginning near 1.777, and ending near 1.779 in a Hopf bifurcation that produces 37 small ellipses. Clearly these ellipses cannot all lie on a single closed curve that does not intersect itself. Chaos therefore appears to be imminent. A high-resolution search reveals a still narrower window of period 208, beginning near 1.7848 and ending near 1.7849 in a period-doubling bifurcation. Again, the period doubling is topologically inconsistent with an invariant closed curve that passes through the 208 points before the bifurcation, and deforms itself continuously into a similar curve passing through the 416 points after the bifurcation, unless the curve crosses itself somewhere. Again chaos seems to be imminent.

We find, in fact, that in the semiperiodic band of period 37, i.e., in the range of τ where A consists of 37, or a multiple of 37, disjoint pieces, with each piece mapping onto another piece, there are values of τ, in particular 1.7844, where A consists of 37 chaotic pieces. Likewise, in the band of period 208 there are values of τ, in particular 1.78494, where the 208 pieces of A are chaotic. The band of period 37 actually resembles a compressed copy of the whole of fig. 2(a), and contains its own semiperiodic bands and periodic windows, some of which may end in Hopf or period-doubling bifurcations, so that chaos may first appear in a band within a band, or even a band within a band within a band.... A precise determination of τ_b may therefore be impractical.

In passing we note that the band of period 37 extends beyond 1.785, so that at 1.785 there is, in addition to the chaotic attractor of fig. 3(c), a second attractor consisting of $407 = 11 \times 37$ points. Points chosen randomly in the area covered by fig. 3(c) appear more likely to be attracted to the chaotic attractor.

Similar routes to chaos, with different details, may be expected for other values of a near 0.36. When $a > 0.5$, $\tau_a < 1$, and, when a is large enough, $\tau_b < 1$ and $\tau_c < 1$, so that C lies above Y^*, and the onset of chaos depends upon other factors. Whitehead and MacDonald [8] have analyzed the case $a = 3$, which seems rather typical. They note that when A expands upward across Y^* it must also cross Y, and the continual crossing and recrossing of Y by an orbit will occur chaotically, much as in the case of eqs. (9). They point out also that the unstable manifold of the origin O, which is attracted to A, must intersect the stable manifold, which consists of Y and its inverse images, so that homoclinic points are produced. Fig. 9 contrasts a two-sided attractor where $\tau > 1$ with one where $\tau < 1$. For the latter, which resembles the Whitehead–MacDonald attractor, the outer boundary is formed by the unstable manifold of O, and negative values of y do not occur.

Does homoclinicity play a role in the case that we have analyzed? Certainly the stable and unstable manifolds of O do not intersect, while Q and Q' have no stable manifolds. It seems possible that a periodic sequence of some period n may lie within A, in which case the nth iterate of eqs. (13) should possess hyperbolic fixed points, whose stable an unstable manifolds should intersect transversally. Such an occurrence would seem to be an effect of the intersections of A with C rather than a cause, if indeed it is possible to separate cause from effect.

We note finally that for $a < 1/8$ the roots of the characteristic equation (15) are real, and $\tau_a = [1 - (1 - 8a)^{1/2}]/(2a)$. At least in the cases that we have examined numerically, computational in-

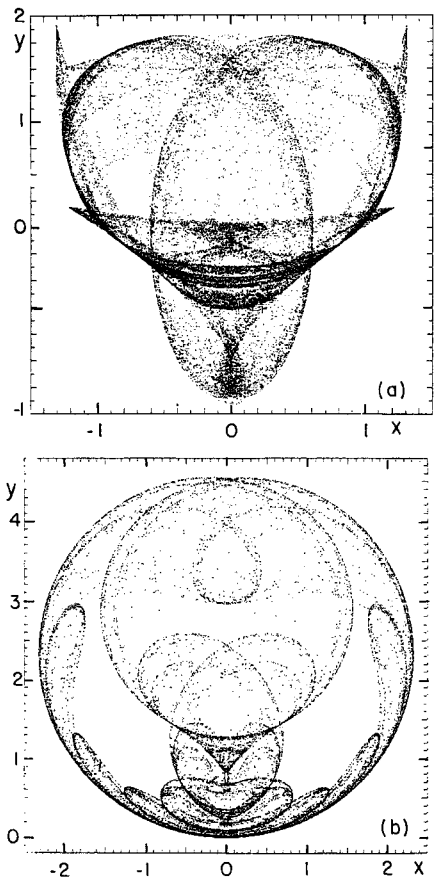

Fig. 9. (a) The attractor of eqs. (13), with $a = 0.6$ and $\tau = 1.5$. (b) The same as (a), except that $a = 1.25$ and $\tau = 0.72$.

stability sets in as soon as $\tau > \tau_a$, so that $\tau_c = \tau_a$, and computational chaos does not occur.

4. A route to computational instability

Every orbit of the differential system (10) is attracted to a fixed point, but, for any positive value of τ in (13), some orbits escape to infinity. As τ increases and A eventually expands, its basin of attraction B contracts. The limit τ_c of computational stability has been reached when A and the boundary of B meet each other.

For the case $a = 0.36$ we can say more. Fig. 10 shows basins B for $\tau = 1.5$ and $\tau = 2.03$, determined numerically by randomly selecting points and seeing what happens to their iterates. The

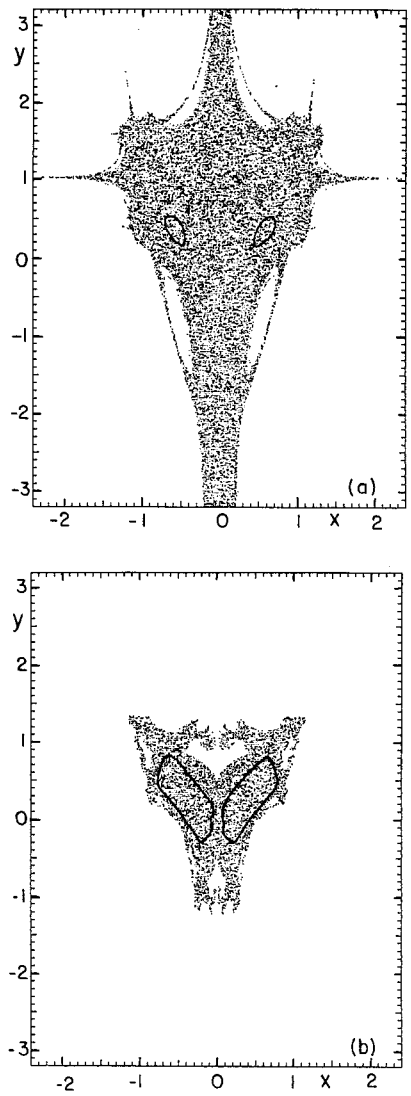

Fig. 10. (a) The combined basin of attraction (shaded region) of A and its image A' in the y-axis, for eqs. (13) with $a = 0.36$ and $\tau = 1.50$. The small quasi-ellipses are A and A'. (b) The same as (a), except that $\tau = 2.03$, and the closed curves are the outer boundaries of A and A'.

basins have some features in common, but they differ in an important respect. For $\tau < 2$, all points on Y are attracted to O, whence B includes a region about Y that becomes increasingly narrow as $y \to \infty$. Likewise B includes regions surrounding the inverse image Y^* of Y and the successive inverse images of Y^*, all extending to infinity.

Some of these are partially resolved in fig. 10(a). For $\tau > 2$, points on Y are attracted to infinity, whence B excludes a region about Y that becomes increasingly narrow as $y \to 0$. Likewise B excludes regions surrounding Y^* and its inverse images. By and large these are too narrow to be resolved in fig. 10(b).

When τ slightly exceeds 2, A still looks much as in fig. 3(d), with smooth boundaries. (For $\tau = 2$ exactly, A, although still chaotic, is degenerate.) As τ increases further, computational instability must set in when A expands upward to meet the very narrow strip enclosing Y^*, and hence just before A meets Y^*, assuming that it has not already set in because A has met the boundary of B somewhere else. Except within periodic windows, the uppermost part of A still lies on the third image of C, so that τ reaches τ_c just before this image becomes tangent to Y^*. One can actually formulate the condition for this tangency as the condition that a readily determined fifth-degree equation in y has two equal roots; this leads to an awkward equation in τ whose solution seems intractable except numerically.

Numerical solutions of (13) indicate that $\tau_c = 2.073$ when $a = 0.36$. As a increases, τ_c becomes smaller, and one finds that τ_c reaches 2.0 when $a = (2z^3 - z^2 - z - 1)/(2z^2 + 2)$, where z is the positive root of the equation $4z^2(z^2 - 1)^4 - (z^2 + 1)^3 = 0$; thus $a = 0.376$. For larger values of a the tangency occurs when $\tau < 2$, so that points on Y^* do not escape to infinity. The attractor becomes two-sided, and other considerations determine τ_c.

5. A system with a limit-cycle attractor

Although numerical determination of a transient time-dependent orbit is often the easiest, if not the most economical, means of locating a fixed-point attractor, numerical integration is probably more often applied to systems whose general solution is expected to be unsteady. Whereas the approximation (2) correctly identifies the stable fixed points of (1) as fixed points, and falsifies only their stability, it generally replaces a time-dependent attracting orbit by a different orbit. The simplest unsteady attracting orbits of equations like (1) are limit cycles.

For our second example we choose the system

$$dx/dt = ax - cy - (ax^2 + by^2)x, \tag{21a}$$

$$dy/dt = cx + by - (ax^2 + by^2)y, \tag{21b}$$

where $a + b > 0$, $a \geq b$, and $c > (a - b)/2$. All orbits except the fixed point at the origin are attracted to the unit circle, as is evident when eqs. (21) are transformed to polar coordinates, and points that have virtually reached the circle continue to move counterclockwise about it, but, unless $b = a$, at a variable speed. We may therefore anticipate that, when (21) is approximated by difference equations, values of τ that are small enough to give rather accurate results on the slowly traveled portions of the circle may be too large to accommodate the rapidly traveled portions, and the non-uniform falsification will cause first a stretching of the circle into an ellipse and then more pronounced distortions.

We shall scale t to make $a = 1$, and treat the case $b = 0$, $c = 1$, so that (21) reduces to

$$dx/dt = x - y - x^3, \tag{22a}$$

$$dy/dt = x - x^2y, \tag{22b}$$

and the first-order approximation becomes

$$x_{n+1} = (1 + \tau)x - \tau y - \tau x^3, \tag{23a}$$

$$y_{n+1} = \tau x - y + \tau x^2 y. \tag{23b}$$

A 180° rotation about the origin leaves the systems unchanged.

Fig. 11 shows the variations of l_1 and l_2 with τ. The figure is somewhat like the portion of fig. 2 where $\tau > \tau_a$. There is a long limit-cycle range, with the inevitable periodic windows, followed by considerable chaos between $\tau_b = 0.475$ and $\tau_c = 0.592$. Fig. 12 is the counterpart of fig. 3, and shows four attractors. In the first the circle is simply elongated. In the second it also possesses

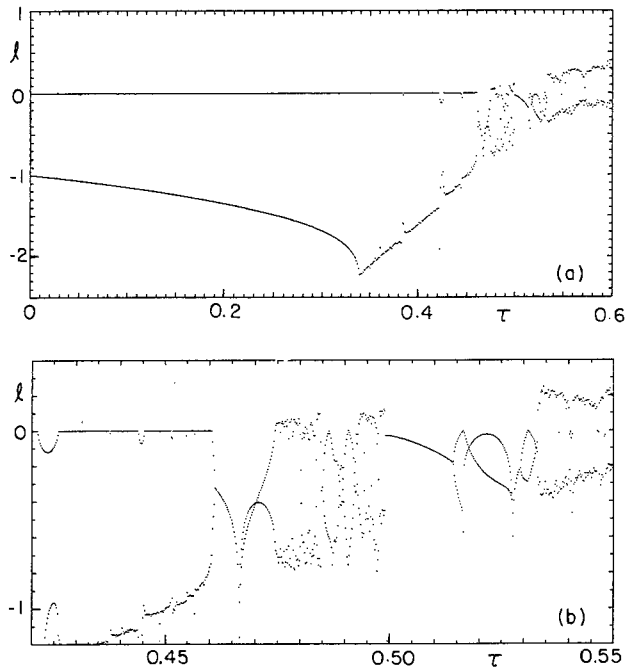

Fig. 11. (a) Numerically estimated values of l_1 and l_2 for values of τ from 0 to τ_c (= 0.592) at intervals of 0.001, for eqs. (23). (b) The same, except for values of τ from 0.42 to 0.55 at intervals of 0.0002.

pronounced kinks, which gave way to loops in the third, which is chaotic. Almost the entire range of τ between figs. 12(b) and 12(c) is occupied by a single window of period 14, and apparently the invariant closed curve ceases to exist somewhere within this range. The fourth attractor, near τ_c, exhibits some of the features of fig. 3(d).

Just as with eqs. (13), there is a critical curve C (no longer a parabola) where the Jacobian of the mapping (23) vanishes, and it possesses an image D that acts as a partial barrier to the spread of A. Fig. 13 shows enlargements of portions of figs. 12(b) and 12(c) along with segments of C and D. As before, a protuberance in the limit-cycle case, and a loop in the chaotic case, are tangent to D, and the loop reveals some substructure. The crossing point in the loop possesses two inverse images in A. Again the importance of homoclinicity is unclear.

Also as before, an irregularly shaped basin of attraction of A contracts as A expands, until computational instability sets in. There seem to be no obvious curves that play the same role that Y and its inverse images play in the earlier example.

6. Higher-order differencing schemes

The results so far obtained may have limited relevance for practical computation, since ordinarily we do not use first-order differencing schemes when seriously seeking the solutions of differential equations. When we turn to higher order, we are faced with a choice of schemes. Commonly used methods for proceeding from a single time to a subsequent time include truncated Taylor-series (TS) schemes and Runge-Kutta (RK) schemes.

Taylor-series expansions in τ of solutions of polynomially nonlinear systems such as (10) and (22) ordinarily have finite radii of convergence, except at fixed points. We may therefore anticipate that if the original differential-equation sys-

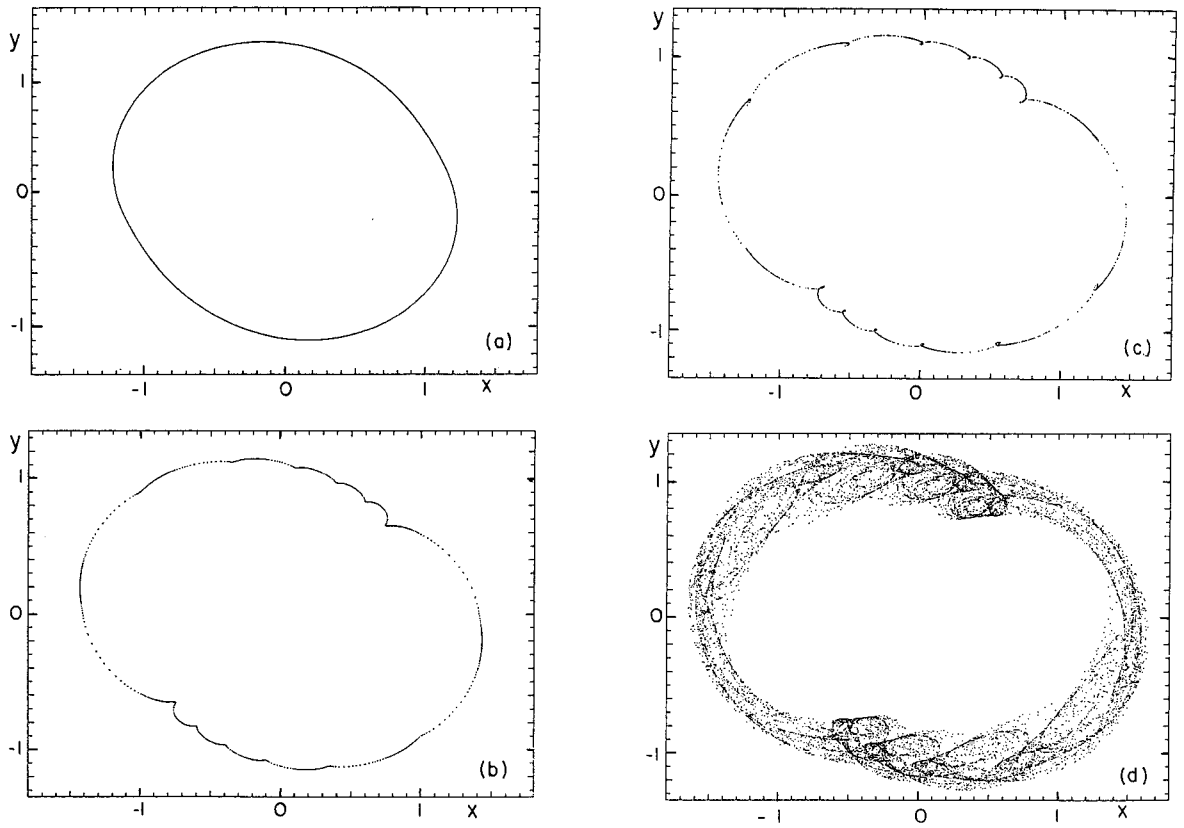

Fig. 12. (a) The attractor of eqs. (23) with $\tau = 0.30$. (b) The same as (a), except that $\tau = 0.46$. (c) The same as (a), except that $\tau = 0.475$. (d) The same as (a), except that $\tau = 0.56$.

tem has a limit cycle as its single attractor, some weighted average τ_0 of the radii of convergence at the points of the limit cycle will act as a limit, as $N \to \infty$, of the value of τ_c for an Nth-order TS scheme. We can also anticipate that if N is large, values of τ slightly below τ_0 will yield good approximations to the limit cycle, while those slightly above τ_0 will produce computational instability. The chaotic range of τ should therefore be very narrow, if it exists at all. Similar reasoning does not apply to a Runge-Kutta scheme, which more nearly resembles a succession of first-order approximations.

Fig. 14 shows the behavior of l_1 and l_2 when the fourth-order TS and the "standard" fourth-order RK schemes are applied to eqs. (22). In the former case, τ_c is only slightly greater than with the first-order scheme, and chaos is rather scarce. In the latter case, τ_c is more than twice as large as in the former, and there is a fairly extensive chaotic range. Fig. 15(a) shows the attractor produced by the RK scheme when $\tau = 0.91 = \tau_c/2$. The curve is smooth, and is not elongated as in fig. 12(a), but as a drawing of a circle it leaves much to be desired. Figs. 15(b) and 15(c) show two attractors when τ is near τ_c. The latter in particular bears no resemblance to the cirlce that it is suppose to approximate.

Somewhat different arguments apply to Nth-order TS schemes when the attractor of the original system is a fixed point Q. Here the radius of convergence at a point P increases without limit as $P \to Q$. As N increases, the limiting value τ_a of τ for which Q is stable increases approximately linearly instead of approaching a limit, so that just beyond the bifurcation at τ_a, if N is large, a very

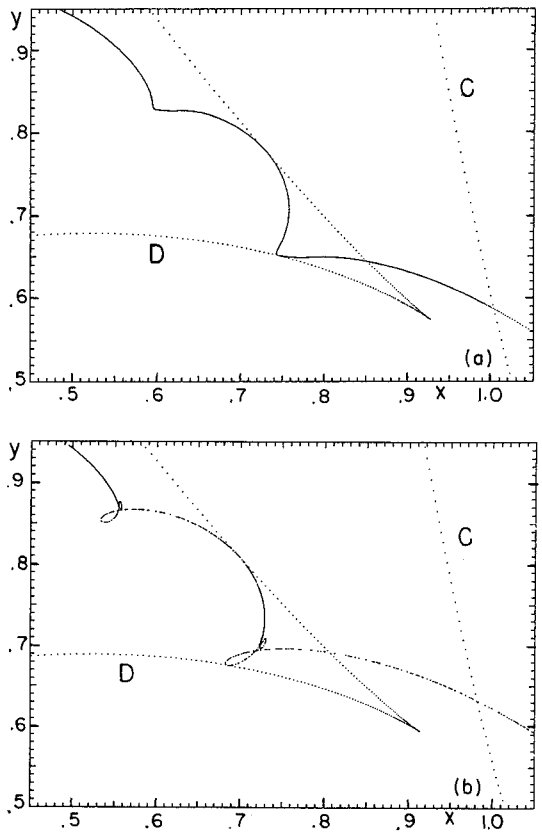

Fig. 13. (a) An enlargement of a portion of fig. 12(b), and portions of the curves C and D. (b) The same as (a), except a portion of fig. 12(c).

slight increase in τ will expand the attractor to points with smaller radii of convergence than τ_a, i.e., τ_c will be reached. Again the chaotic range, if it exists, will be very narrow.

For eqs. (10), τ_a is simply the value of τ that makes the Taylor-series expansion of $e^{\lambda\tau}$, truncated to the τ^N term, have an absolute value of unity, where λ satisfies the characteristic equation (12) with x and y assuming their values on Q or Q'. The discrepancy between the values of τ_c when the two fourth-order schemes are applied to (10), with $a = 0.36$, is less spectacular than with (22), but qualitatively similar.

We encountered a peculiar phenomenon when applying the third-order TS scheme to eq. (10). After computational instability sets in, a further increase in τ renders the scheme computationally stable again. Unlike the first-order scheme, a higher-order scheme can introduce new fixed points, and here these points prove to be stable in a range of τ that does not overlap the range where Q and Q' are stable.

7. Concluding remarks

When one seeks approximate solutions of a set of differential equations by stepwise numerical integration, the choice of a time increment τ small enough to ensure computational stability, but still not very small, may yield chaotic solutions, even when the true solutions approach limit cycles or fixed points. We have examined some aspects of this computational chaos. In two simple selected systems we have found that chaos first sets in when an attractor acquires two distinct points that map to the same point. This in turn occurs when the slope of an intersection of the attractor with the critical curve, in a rectifying coordinate system, changes its sign. Other factors can determine the onset of computational chaos in other systems.

Different schemes, even if they have the same order, may yield considerably different results. A Runge-Kutta scheme may produce chaos over a considerable range of τ where a Taylor-series scheme would produce computational instability. In some instances a further increase in τ after computational instability has set in can bring about a temporary return to computational stability.

Despite the variety of phenomena that we have considered, our scope has been limited. We have not examined what can happen when the true solution of the differential system is chaotic. The computational scheme might produce more intense chaos, or chaos with a higher fractional dimension, but it might also replace the chaos by a limit cycle or a periodic solution. We also have not considered what happens when other types of differencing scheme, some of which are designed to be absolutely stable, are used. Perhaps more importantly, we have not examined systems with

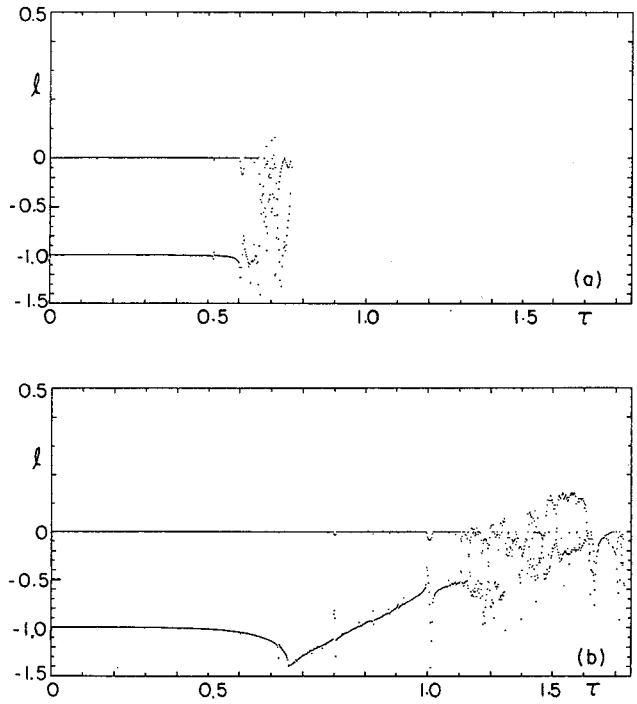

Fig. 14. (a) Numerically estimated values of l_1 and l_2 for values of τ from 0 to τ_c ($= 0.77$), at intervals of 0.002, when a fourth-order Taylor-series scheme is applied to eqs. (22). Note the stretched scale for $l > 0$. (b) The same as (a), except that a fourth-order Runge-Kutta scheme is applied to eqs. (22), and $\tau_c = 1.82$.

more than two variables, where the possible non-chaotic attractors include tori.

Computational chaos is but one instance of chaos or other interesting behavior that has been produced, intentionally or inadvertently, by carrying out standard computation procedures without following all of the directions. Other examples include the wild oscillations that can occur when Newton's method is used as one would use it to solve an algebraic equation, only without the restriction that the initial approximation be a good one [16].

One may wonder whether computational chaos is of much importance for practical numerical integration. In working with a simple system one can generally afford to avoid it by making τ very small. When a system has many variables, however, economy may demand a larger τ. We have demonstrated one system where, with a fourth-order Runge-Kutta scheme, which one might assume would become rapidly more accurate as τ decreases, finding a value of τ yielding computational stability and then cutting this value in half will still not produce a very good approximation.

A special situation arises in meteorology, where the systems of equations used in weather forecasting may have thousands or even hundreds of thousands of variables, and where their solutions may represent the familiar migratory storms, with time scales on the order of days, and superposed smaller-amplitude oscillations with time scales of a few hours. Often we are interested only in the slower variations, and we tend to feel that, if we have chosen τ just small enough to avoid the computational instability that the faster oscillations would otherwise produce, the solutions will serve our needs. The present work suggests that with this choice of τ the faster oscillations may

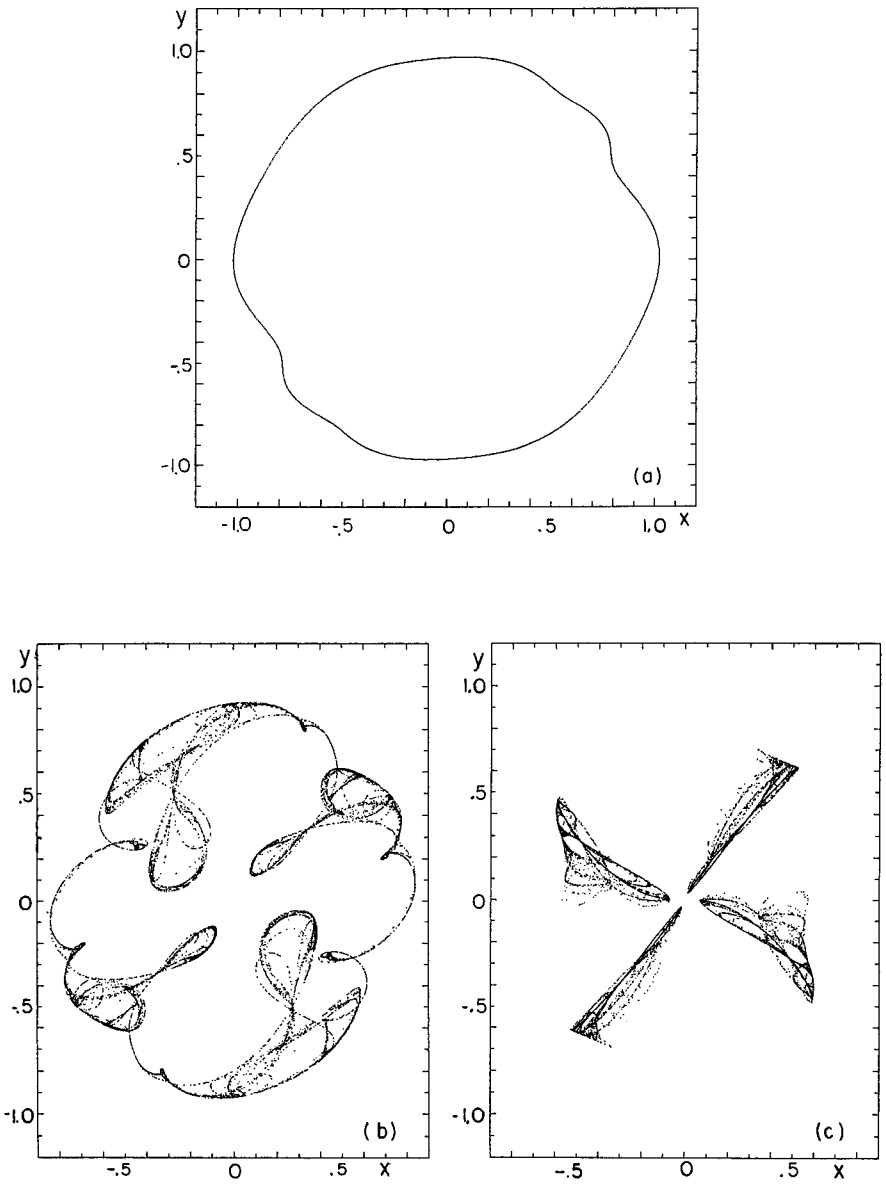

Fig. 15. (a) The attractor A when a fourth-order Runge-Kutta scheme is applied to eqs. (22), with $\tau = 0.91$. (b) The same as (a), except that $\tau = 1.6$. (c) The same as (a), except that $\tau = 1.7$.

become chaotic, or, if they should be chaotic anyway, they may become more strongly chaotic or perhaps not chaotic at all. If there is then appreciable coupling between the faster and slower variations, the general behavior of the entire solution may be suspect. Similar situations can probably be cited throughout the sciences, since multiple-time-scale phenomena appear to be ubiquitous.

Quite apart from its possible influence on practical numerical integration, computational chaos may produce a virtually endless variety of strangely shaped attractors. More importantly, systems

exhibiting computational chaos can serve as illustrative cases in studies of the properties of noninvertible mappings.

Acknowledgements

This work has been supported by the Climate Dynamics Program of the Division of Atmospheric Sciences, National Science Foundation, under Grant ATM 85-15010. I wish to thank V. Krishnamurthy for his many helpful comments, and I wish to thank two anonymous reviewers for some valuable suggestions.

References

[1] N.A. Phillips, An example of non-linear computational instability, in: The Atmosphere and the Sea in Motion, B. Bolin, ed. (Rockefeller Inst. Press, New York, 1959), p. 501.
[2] T.-Y. Li and J.A. Yorke, Period three implies chaos, Am. Math. Mon. 82 (1975) 985.
[3] J. Guckenheimer, On the bifurcation of maps of the interval, Invent. Math. 39 (1977) 165.
[4] P. Collet and J.-P. Eckmann, Iterated Maps on the Interval as Dynamical Systems (Birkhäuser, Boston, 1980).
[5] P.R. Stein and S.M. Ulam, Non-linear transformation studies on electronic computers, Rozprawy Mat. 39 (1964) 1.
[6] M. Yamaguti and S. Ushiki, Chaos in numerical analysis of ordinary differential equations, Physica D 3 (1981) 618.
[7] M. Hénon, A two-dimensional mapping with a strange attractor, Commun. Math. Phys. 50 (1976) 69.
[8] R.R. Whitehead and N. MacDonald, A chaotic mapping that displays its own homoclinic structure, Physica D 13 (1984) 401.
[9] J.M. Burgers, Mathematical examples illustrating relations occurring in the theory of turbulent fluid motion, Akad. Vetens. Amsterdam 17 (1939) 1.
[10] M. Yamaguti and H. Matano, Euler's finite difference scheme and chaos, Proc. Jap. Acad. A 55 (1979) 78.
[11] S. Ushiki, Central difference schemes and chaos, Physica D 4 (1982) 407.
[12] E.N. Lorenz, Deterministic nonperiodic flow, J. Atmos. Sci. 20 (1963) 130.
[13] J. Guckenheimer and P. Holmes, Nonlinear Oscillations, Dynamical Systems, and Bifurcations of Vector Fields (Springer, New York, 1983).
[14] R.L. Devaney, An Introduction to Chaotic Dynamical Systems (Benjamin/Cummings, Menlo Park, CA, 1986).
[15] J.R. Beddington, C.A. Free and J.H. Lawton, Dynamic complexity in predator–prey models framed in difference equations, Nature 255 (1975) 58.
[16] J.H. Curry, L. Garnett and D. Sullivan, On the iteration of a rational function, Commun. Math. Phys. 91 (1983) 267.